Molecular Physics
Vol. 110, No. 5, 10 March 2012, 267–276

Taylor & Francis
Taylor & Francis Group

RESEARCH ARTICLE

Molecular dynamics simulation of a graphite-supported copper nanocluster: thermodynamic properties and gas adsorption

S. Jalili[ab]*, C. Mochani[a], M. Akhavan[b] and J. Schofield[c]

[a]*Department of Chemistry, K. N. Toosi University of Technology, P. O. Box 15875-4416, Tehran, Iran;* [b]*Computational Physical Sciences Research Laboratory, School of Nano-Science, Institute for Research in Fundamental Sciences (IPM), P.O. Box 19395-5531, Tehran, Iran;* [c]*Chemical Physics Theory Group, Department of Chemistry, University of Toronto, 80 Saint George Street, Toronto, Ontario, Canada M5S 3H6*

(*Received 2 September 2011; final version received 9 November 2011*)

Molecular dynamics simulations were conducted for a cubic Cu cluster supported on a graphite bilayer. The Sutten–Chen and Lennard–Jones potentials were used for metal–metal and metal–graphite interactions, respectively. Heating and cooling processes were performed by NVT simulations at different temperatures in the range 200 to 1800 K. The melting point was identified on the basis of caloric and heat capacity curves. The calculated melting point was 770 K, far below the bulk melting point of crystalline copper. Several phenomena such as the appearance of a hysteresis (irreversibility) in caloric curves, surface melting, and cluster-induced surface wetting were justified from the results. The simulation of cluster in the presence of gas atmosphere showed that the CO gas is adsorbed more than H_2 and it has a greater impact on the cluster's structure.

Keywords: molecular dynamics; copper cluster; graphite-supported nanocluster; gas adsorption; melting

1. Introduction

Copper nanoclusters supported on graphite and metal oxide surfaces have found many applications in heterogeneous catalysis [1]. In recent years, much attention has been paid to the melting behaviour and thermodynamic properties of Cu and other transition metal nanoclusters. The melting point of metal nanoclusters is strongly dependent on their size. It is normally much below the bulk melting point and decreases with cluster size [2]. This is because of a large fraction of surface atoms in small clusters.

Molecular dynamics (MD) simulation is a useful tool for a detailed understanding of the properties of nanoclusters. The melting points of Cu clusters with different sizes and shapes have been obtained by molecular dynamics simulations using an embedded-atom model (EAM) [3] and tight-binding [4] potentials. Molecular dynamics methods have been also employed to study the thermodynamic properties and diffusivity of supported pure and bimetallic nanoclusters [5–9].

The adsorption of gases on supported nanoclusters is a topic of major interest because of its importance in catalysis and corrosion. The CO gas adsorbed on copper electrodes leads to partial passivation of the electrode, which decreases the H_2 evolution current [10]. Many experimental and theoretical studies have been performed to understand the energetic of gas adsorption and its effect on the shape of copper clusters [11–13]. The effect of oxygen [14] and inert gas [15] adsorption on supported platinum clusters has also been studied using MD simulations. Here, we report MD simulation studies of the melting behaviour of a cubic Cu cluster supported on a static graphite surface. Furthermore, the effect of CO and H_2 adsorption on the Cu cluster at different temperatures is investigated.

2. Computational details

2.1. *Potential functions and parameters*

Cu–Cu interactions were modelled using the Sutton–Chen (SC) potential [16], which is a convenient model to study metal clusters with fcc structure, because the local density effects is included in its parameterization. The potential energy in the SC model is:

$$U_{\mathrm{tot}} = \varepsilon\left[\frac{1}{2}\sum_{i\neq j}\sum_{j}\left(\frac{a}{r_{ij}}\right)^{n} - c\sum_{i}\rho_i^{1/2}\right] \qquad (1)$$

The first term is a pair repulsion potential and the second term represents the metallic bonding energy associated with the local density ρ_i, which is calculated

*Corresponding author. Email: sjalili@kntu.ac.ir

ISSN 0026–8976 print/ISSN 1362–3028 online

http://dx.doi.org/10.1080/00268976.2011.640953
http://www.tandfonline.com

as follows:

$$\rho_i = \sum_{j \neq i} \left(\frac{a}{r_{ij}}\right)^m \quad (2)$$

where r_{ij} is the distance between atoms i and j, c is a dimensionless parameter, and ε and a are parameters with dimensions of energy and length, respectively. For Cu–Cu interactions, the values chosen were $\varepsilon = 0.012386$ eV, $a = 3.61$ Å, $c = 39.755$, $m = 6$, and $n = 9$ [6].

The Lennard–Jones potential with $\varepsilon = 0.019996$ eV and $\sigma = 3.225$ Å was used for Cu–C interactions, which is obtained from the available Cu–Cu [17] and C–C [18] parameters, using the Lorentz–Berthelot mixing rules.

CO and H_2 gases were considered as two-site models with a fixed interatomic distance of 0.746 Å for H_2 [19] and 1.163 Å for CO [20]. Their Lennard–Jones energy and length parameters and charges are shown in Table 1.

2.2. *MD procedure*

Classical MD simulations were performed on a 256-atom cube-shaped copper cluster with fcc structure, supported on a model graphite surface. The graphite was modelled as two carbon layers in ABAB arrangement with dimensions of $49.2 \times 42.6 \times 6.8$ Å^3 and 1600 carbon atoms. The cluster was placed 3 Å above the graphite surface (Figure 1). The graphite layers were kept rigid and constant during simulations and the periodic boundary conditions were applied only in x and y directions.

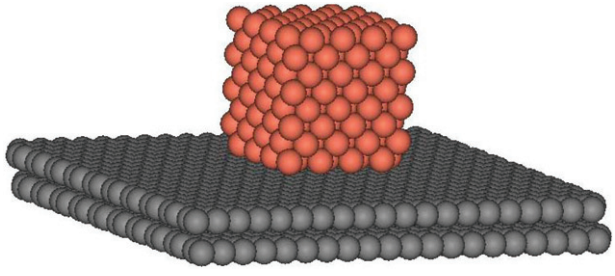

Figure 1. Initial structure of the graphite-supported copper cluster.

Table 1. Potential parameters for CO and H_2 gases [19,20].

	ε (eV)	σ (Å)	q (e)
H	0.003179	2.92	0
C	0.004553	3.43	+0.107
O	0.002601	3.12	−0.107

A set of simulations were performed at various temperatures in the range 200 to 1800 K to heat the system. Simulations were done in NVT ensemble using the DL_POLY 3.10 [21] software. Temperature was kept constant using the Evans thermostat [22]. Equations of motion were integrated by a leap-frog method, with a time step of 1 fs. At each temperatures, the system was first equilibrated for 400 ps, followed by 200 ps of production run. Similar simulations were performed to cool the system from 1800 K back to 200 K.

In the second stage, simulations were performed to study the effect of a gaseous atmosphere of H_2 or CO on the supported Cu cluster. The initial simulation box was composed of the cubic cluster on graphite bilayer, together with 400 gas molecules at random positions. The box was a parallelepiped with dimensions $49.2 \times 42.6 \times 60.0$ Å^3 and periodic in all three directions. Four temperatures (200, 400, 600, and 800 K) were chosen for this stage. Various gas pressures at constant volume and temperature were created by changing the number of gas molecules. For this purpose, the pressure was reduced near to vacuum in several steps. At each step, 40% of gas molecules were removed and after the end of each simulation, its output was used as input for the next step. For both H_2 and CO, the simulation with maximum number of gas molecules was performed for 1100 ps (800 ps equilibration and 300 ps production) and subsequent (lower-pressure) simulations were performed for 400 ps (100 ps equilibration and 300 ps production). Other conditions were similar to the first stage.

The analysis of simulated trajectories and calculation of different properties were performed using the utilities of dlpoly program, as well as the Gromacs 4.0 [23] simulation package. The distance criterion for counting the number of adsorbed molecules in the second stage was chosen from the position of the first peak in radial distribution function for the gas molecules around the cluster. This was 2.85 Å for H_2 and 3.90 Å for CO.

3. Results and discussion

3.1. *Thermodynamic properties*

A caloric curve (potential energy vs. temperature) is obtained by heating the system from 200 to 1800 K and then cooling it back to its original temperature. Figure 2(a) shows such a curve for the cubic 256-atom Cu cluster. The calculated potential energy has contributions from metal–metal and metal–graphite

interactions. Calculations show that the interaction energy of metal–graphite is two orders of magnitude larger than the metal–metal interaction energy. A sudden jump in this curve shows a phase transition in the cluster at the corresponding transition temperature. The temperature of the jumps in the heating and cooling curve correspond to melting and freezing points, respectively. Figure 2(a) shows that the temperature range of the phase transition is 700−800 K for heating and 600−700 K for cooling.

At temperatures higher than the melting point, the heating and cooling curves have the same slope and lie on top of each other. In contrast, below the melting point, the curves differ and the heating curve have greater potential energes than the cooling curve. Therefore, a hysteresis is appeared during the cooling process. The presence of such a hysteresis in solid–liquid transitions has been justified theoretically [24] and agrees with similar studies [5,25]. The lower potential energies in the cooling curve means that, with heating and cooling (simulated annealing), metastable states are avoided and a lower-energy state can be achieved.

For a more accurate determination of melting temperatures, the heating simulations were repeated in the temperature range 700−900 K, with 20 K increments.

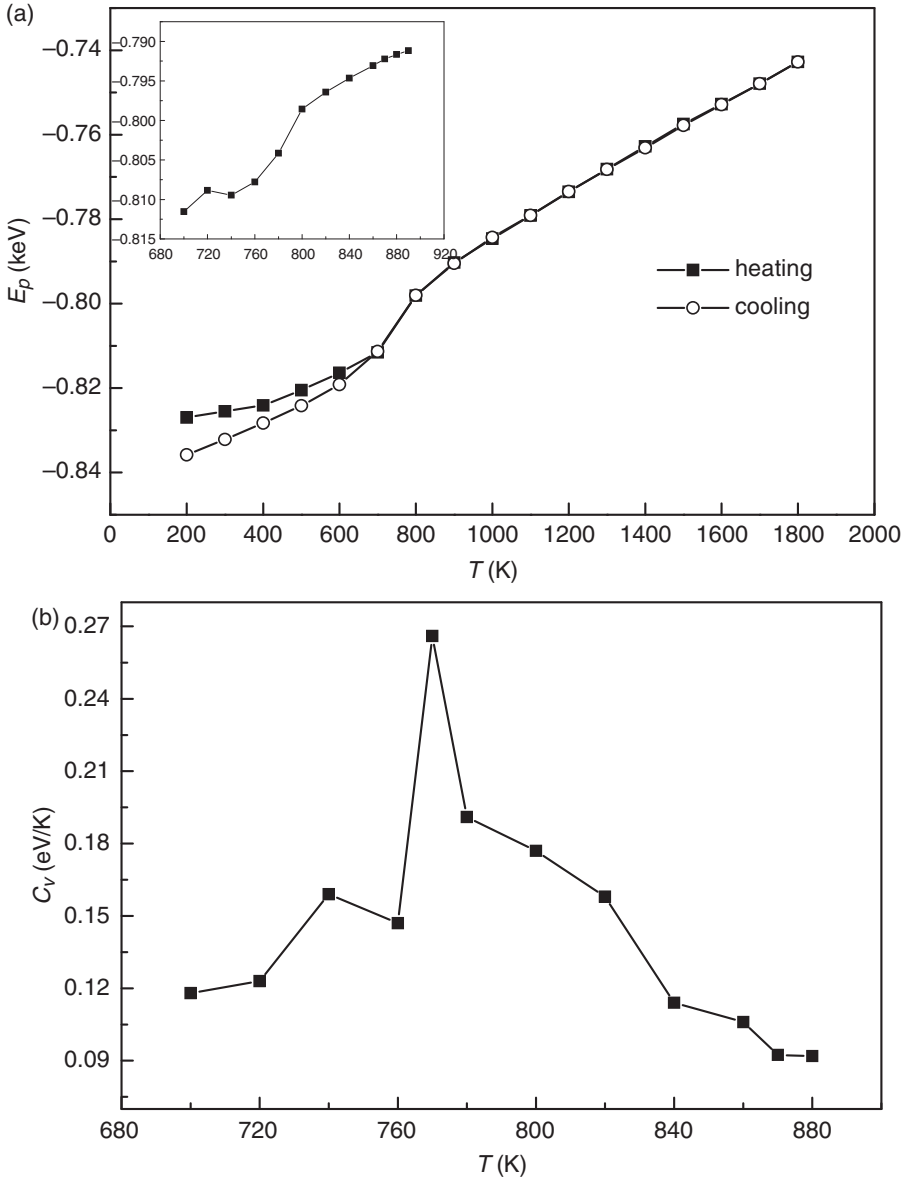

Figure 2. The caloric curve (a) and the heat capacity at different temperatures (b) for heating and cooling processes.

The potential energy vs. temperature for these simulations is shown in the inset to Figure 2(a). The energy jump occurs in the range 750–800 K. The temporary decrease of energy at 740 K, which is probably due to the change to a semi-spherical shape as the result of surface melting and the diffusion of surface atoms. This change has been observed using electronic microscopy [26] and is a hallmark of solid–solid transitions in nanoclusters. Surface melting accounts for the hysteresis between the heating and cooling curves in solid region [5].

By calculating the heat capacity of the nanocluster at constant volume we can determine accurately the melting point. Heat capacity is obtained from the simulated trajectory as follows:

$$C_v = \frac{\left\langle \left(E_p - \langle E_p \rangle\right)^2 \right\rangle}{kT^2} + \frac{3}{2}Nk \tag{3}$$

where N is the number of atoms in the cluster and E_p is the potential energy. Figure 2(b) shows a plot of heat capacity against temperature. This curve shows a first-order phase transition, with the melting point at 770 K. This temperature is much below the experimental melting point of the bulk crystalline copper, which is equal to 1356.15 K [6]. Therefore, we see that the metal clusters have lower melting points than their crystalline lattices.

3.2. *Bond-orientational order parameters*

We can use the bond-orientational order parameters to determine the crystal structure of a nanocluster [27]. In this method, a bond is defined as a vector connecting a pair of adjacent atoms. A cutoff is used to identify the adjacent atoms, a common choice being the minimum distance between the first and second peaks in the Cu–Cu radial distribution function. The local order parameters associated with a bond **r** are:

$$Q_{lm}(\mathbf{r}) \equiv Y_{lm}(\theta(\mathbf{r}), \phi(\mathbf{r})) \tag{4}$$

where $\theta(\mathbf{r})$ and $\phi(\mathbf{r})$ are polar and azimuthal angles of the bond with respect to an arbitrary and constant reference framework, respectively and Y_{lm} are spherical harmonics. By averaging over all bonds in the cluster, it is possible to obtain global bond order parameters:

$$\bar{Q}_{lm} \equiv \frac{1}{N_b}\sum_{1}^{N_b} Q_{lm}(\mathbf{r}) \tag{5}$$

where N_b is the number of bonds. In order to have parameters independent of rotations of the reference framework, the second-order invariants are defined:

$$Q_l \equiv \sqrt{\frac{4\pi}{2l+1}\sum_{m=-l}^{l}\left|\bar{Q}_{lm}\right|^2} \tag{6}$$

Two bond order parameters that are useful for the identification of crystal structures are Q_4 and Q_6. Table 2 shows the characteristic values of these parameters for different types of crystal structures [28]. The icosahedral structure is not periodic, so its bond order parameters should depend on the cluster size.

Figure 3 shows the calculated values of Q_4 and Q_6 for the cluster at different temperatures. According to the position of first minimum on Cu–Cu radial distribution functions, a cutoff value of 3.17 Å was used at 200 K. Similar values were obtained at other temperatures. The initial values of Q_4 and Q_6 correspond to a face-centred cubic (fcc) structure (Table 2), but they rapidly decrease with increasing temperature. This rapid decrease may be attributed to the surface melting. In the temperatures near to melting point, the

Table 2. Bond order parameters for various crystal structures.

Geometry	Q_4	Q_6
Fcc	0.19094	0.57452
Hcp	0.09722	0.48476
Sc	0.76376	0.35355
Bcc	0.08202	0.50083
Liquid	0	0
Ih bulk	0	0.19961
Ih surface	0	0.20729

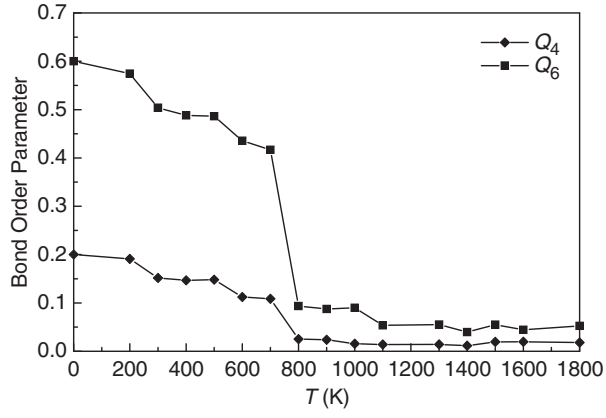

Figure 3. Variations of the bond-orientational order parameters with temperature for the cluster.

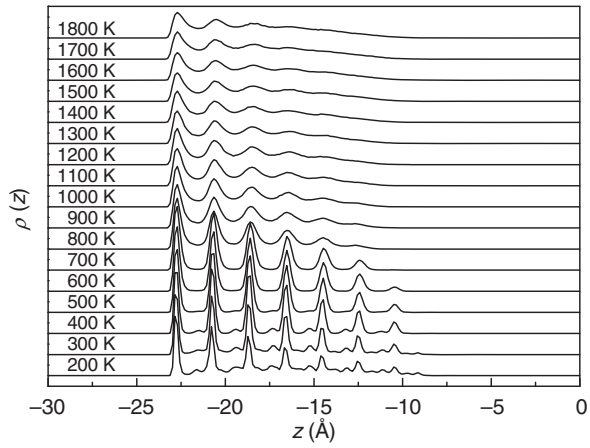

Figure 4. Density profiles, $\rho(z)$, in the direction normal to the graphite surface at different temperatures.

cluster approaches to the hexagonal close packed (hcp) geometry. At melting point (~800 K), the Q_4 parameter abruptly reaches to near zero, which shows the liquid phase. The Q_6 parameters has nonzero values after the phase transition, which is probably due to the layering of cluster on the graphite surface. Similar trends have been observed for other nanoclusters [25,29]. The temperature of abrupt decrease in Q_4 and Q_6 agrees with the melting temperature obtained from the caloric curve.

3.3. *Temperature-dependent variations in cluster structure and shape*

One way to examine the structural changes of the nanocluster during heating and cooling is to use density profiles, $\rho(z)$, which are obtained from the following relation:

$$\rho(z) = \frac{n(z)\sigma^3_{\mathrm{CuCu}}}{\Delta h A_{xy} N_s} \tag{7}$$

where $n(z)$ is the number of Cu atoms in a slice of the simulation box parallel to the xy plane of graphite, with a width Δh. A_{xy} is the surface area of the graphite xy plane, and N_s is the number of samples. Here, we used a value of 0.018 Å for Δh.

Density profiles are plotted at various temperatures in Figure 4, the graphite surface being located at $z = -25.9$. The plots show that the cluster maintains its fcc structure between 300 and 500 K. The interlayer spacing is increased from 1.9 Å at 300 K to 2.1 Å at 600 K. This increase may be a result of the change of cluster structure from fcc to hcp. These findings agree with the results obtained from bond order parameters.

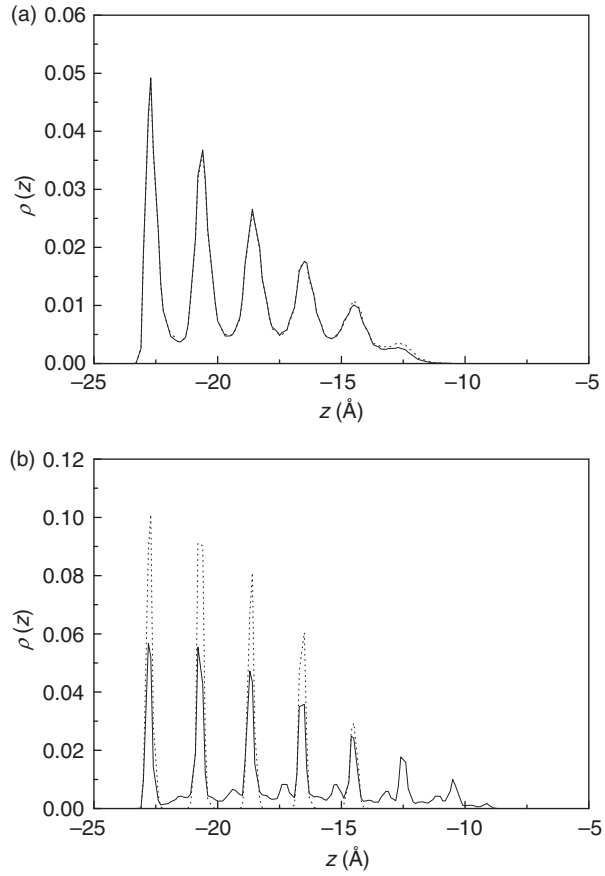

Figure 5. Density profiles at 800 K (a) and 300 K (b) during the heating and cooling processes.

At temperatures between 200 and 600 K, the nanocluster has seven layers, but at 700 K one layer is lost, which shows the structural changes and initiation of melting. Upon gradual increase of temperature further layers disappear and the cluster is in a liquid-like state. The peaks near the graphite surface have significant intensities even at higher temperatures, which is a sign of the temperature-induced wetting phenomenon. The outer peaks disappear at temperatures near the melting point because the surface melting disappears. The surface atoms diffuse and melt, but the inner parts of the cluster still have the properties of solids. Similar changes have been observed in theoretical [5] and experimental [26] studies of cubic Pt nanoclusters.

Further insights may be obtained by comparing density profiles for heating and cooling at a specific temperature. Figure 5 shows such profiles for two temperatures. Despite the slight difference for 800 K (Figure 5(a)), there is a large difference between the two curves at 300 K (Figure 5(b)). In the profiles associated with cooling, the height of peaks near the graphite

surface is larger, so the surface wetting is more in this case. This has been obtained for supported Pt clusters [5] as well. Furthermore, for cooling, the layers are more complete and the density is zero in the spaces between layers. The difference between heating and cooling was examined in caloric curves earlier (Figure 2(a)). The structure and shape of the nanoclusters obtained at 300 K from heating and cooling are different. The cluster obtained from heating from 200 K has seven layers, but in the cooled cluster the number of peaks (or layers) reduces to 5. Figure 6 shows this difference more clearly for the structures obtained at 300 K.

In order to further examine the structural changes, we can make use of a deformation parameter:

$$\eta_q(t) = \frac{1}{N}\sum_{i=1}^{N}\left(\left|q_i(t) - q_{\mathrm{cm}}(t)\right|\right) \tag{8}$$

in which q_i shows x, y, or z coordinates of atom i. Summation is over all atoms of cluster and q_{cm} is the cluster's centre of mass position. η_q shows cluster deformation along the q direction. Using the deformation parameters we can monitor the global changes in cluster's structure.

Figure 7 shows the deformation parameters along three spatial coordinates at various temperatures. At low temperatures, where the nanocluster has a cubic shape, the deformation parameters are almost equal in three directions. With increasing temperature, the parameter along the x axis smoothly increases and along the y axis, it smoothly decreases. At melting point, η_x and η_y are relatively equal, which shows that the cluster has a semi-spherical shape. The cluster contracts along the z axis (normal to the graphite surface) at temperatures near the melting point, so that the η_z is nearly zero at high temperatures. This flattening of the cluster on the support's surface has been observed for alloyed clusters of Cu and Ni [6]. After melting, where the cluster is liquid, its shape does not change significantly. The only exception is for η_y at 1600 K, which shows that the cluster is expanded along the y axis and is due to the atomic motions in liquid state.

3.4. *Dynamic properties of the nanocluster*

The diffusion process is examined by calculating the mean square displacement (MSD) of atoms as a function of time. MSD is obtained from the following relation:

$$\Delta\mathbf{r}(t) = \left\langle\left|\mathbf{r}_i(t+s) - \mathbf{r}_i(t)\right|^2\right\rangle \tag{9}$$

where the averaging is over all the atoms of type i and over the choices of different time origins s. The self-diffusion coefficient is obtained from the time dependence of MSD, using the so-called Einstein's relation:

$$\lim_{t\to\infty}\Delta\mathbf{r}(t) = 6D_i t \tag{10}$$

Figure 8 shows the calculated values of the self-diffusion coefficient at different temperatures. Below 700 K, the cluster has a solid structure, characterized by its constant and nearly zero values of D. At 800 K,

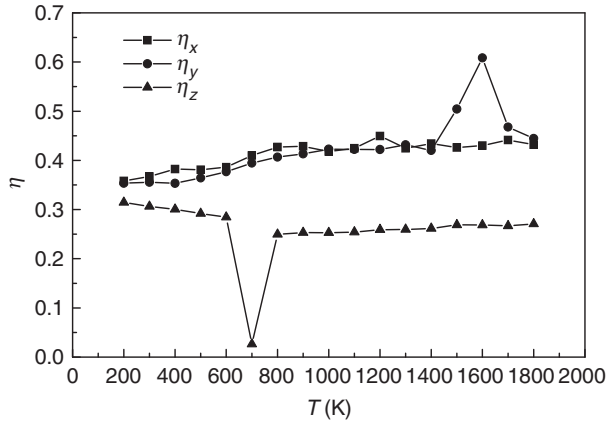

Figure 7. Deformation parameters in three dimensions for the cluster at different temperatures.

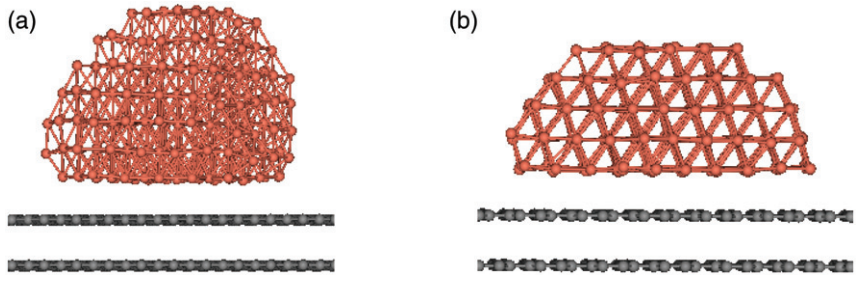

Figure 6. Nanocluster obtained at 300 K from the heating (a) and cooling (b) processes.

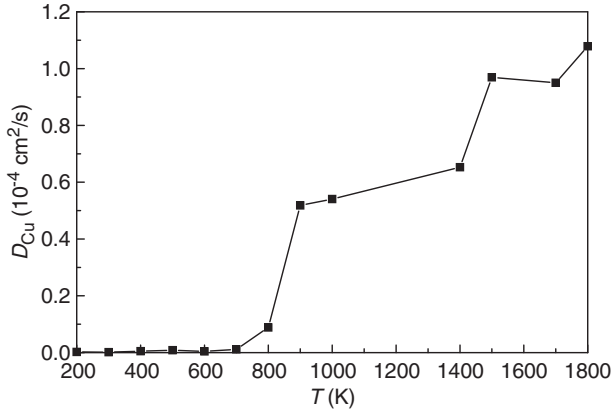

Figure 8. Average value of diffusion coefficient for the cluster during heating.

when the cluster is starting to melt, the self-diffusion coefficient is higher, and at 900 K, it shows a sudden jump to an even higher value. In general, with increasing temperature, the motion of surface atoms and their tendency to diffuse into the interior increases, which reflects in higher values of D. Similar behaviour, which is in accordance with the results obtained from density profiles, has been reported for Pt nanoclusters [5].

3.5. *Adsorption isotherms of H_2 and CO on nanocluster*

Figure 9 shows the adsorption isotherms for H_2 and CO gases on the graphite-supported Cu nanocluster. For this, the number of adsorbed molecules (with the criterion explained in methods) is plotted against the gas pressure at different temperatures. As noted before, the gas pressure was changed by changing the number of molecules at constant volume. The values of pressure were calculated using the van der Waals equation of state.

According to Figure 9, at lower temperatures, more gas is adsorbed, but with rising temperature the number of adsorbed molecules and the slope of the curve decrease. The isotherms correspond to the Langmuir isotherm, type I in IUPAC classification [30], because they saturate after a certain pressure. Comparison of the plots at a specific loading and temperature shows that the amount of CO adsorbed is more than H_2. This is expected, based on the Lennard–Jones energy, and length parameters, but the difference is not so great, because the H_2 molecules are small and can aggregate around the cluster.

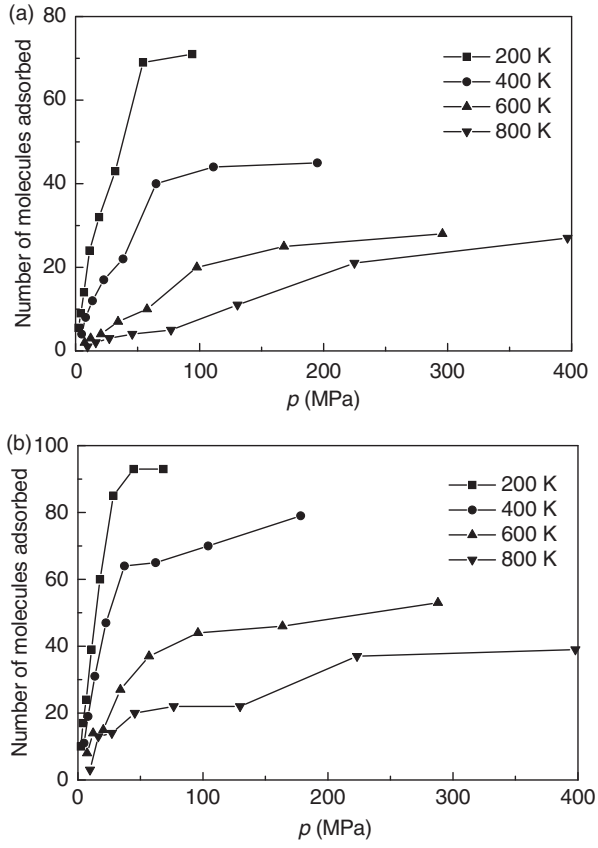

Figure 9. Adsorption isotherms for H_2 (a) and CO (b) gases.

3.6. *Effect of gaseous atmosphere on the nanocluster*

The presence of gas molecules affects the structure and shape of nanoclusters [11,15]. For a nanocluster of a certain size, the effect of gas depends on surface coverage, temperature, and the nature of the gas itself. Figure 10(a)–(c) (top) shows the clusters obtained from the simulation in vacuum, and in the presence of 400 molecules of H_2 and CO at 400 K. The gas molecules have been deleted for clarity. The nanocluster in vacuum (Figure 10(a)) has a layered structure, and in the presence of gas molecules, the pressure of gas induces an expansion in the z direction, perpendicular to the graphite surface. When the pressure is gradually reduced to near vacuum (Figure 10(d), (e)), the nanocluster adopts a structure which is not similar to the configuration obtained for the simulation in vacuum (Figure 10a). It seems that the gas molecules have made irreversible changes in the cluster and the cluster maintains the stable structure obtained in the presence of higher amounts of gases. Similar irreversibility has been observed for the adsorption of inert gases on graphite-supported platinum clusters [15].

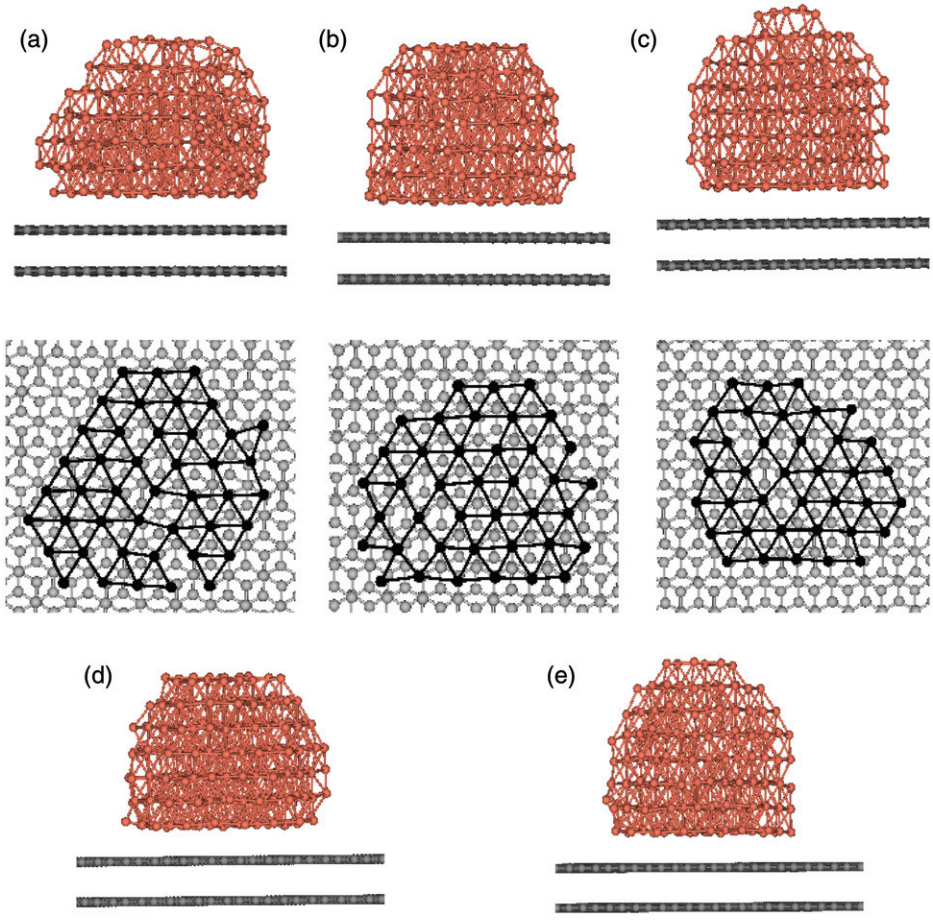

Figure 10. Structure of the cluster (top) and the layer adjacent to graphite surface (bottom), obtained for the simulation at 400 K in vacuum (a), with 400 H_2 molecules (b), and with 400 CO molecules (c). Also shown are the cluster structures in the vacuum obtained from the gradual removal of H_2 (d) and CO (e) molecules.

Figure 10 shows that in the case of CO, and not H_2, the number of layers increases. The density profiles in the z direction for these systems are shown in Figure 11. For simulation with CO gas a further peak appears, which shows a new layer of Cu atoms. The cluster has eight layers in the presence of CO molecules.

Comparison of the layer adjacent to the graphite surface (Figure 10, bottom) shows that the presence of gas leads to a deformed and smaller layer. Some Cu atoms in this layers are in curved lines in order to increase the interactions between the graphite surface and adsorbed gas molecules. All these accommodations facilitate interactions in the system.

The effect of gas atmosphere on the nanocluster is also temperature-dependent. Figure 12 shows the mean square displacement (MSD) as a function of simulation time (the linear region) for simulations at two different temperatures in vacuum, with 400 CO, and with 400 H_2 molecules. At 200 K (below the cluster's melting point), the MSD plot has a small slope

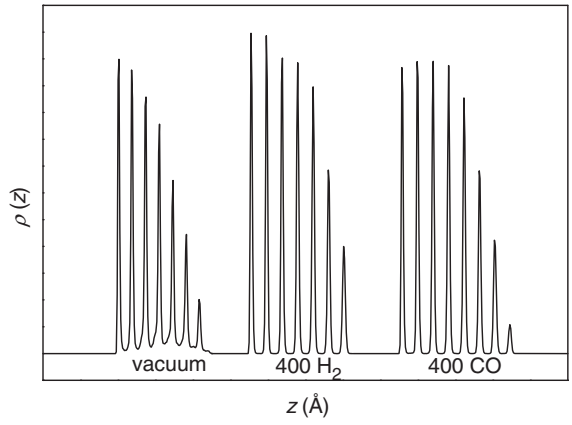

Figure 11. Density profiles at 400 K for the cluster in vacuum, with 400 H_2 molecules, and with 400 CO molecules.

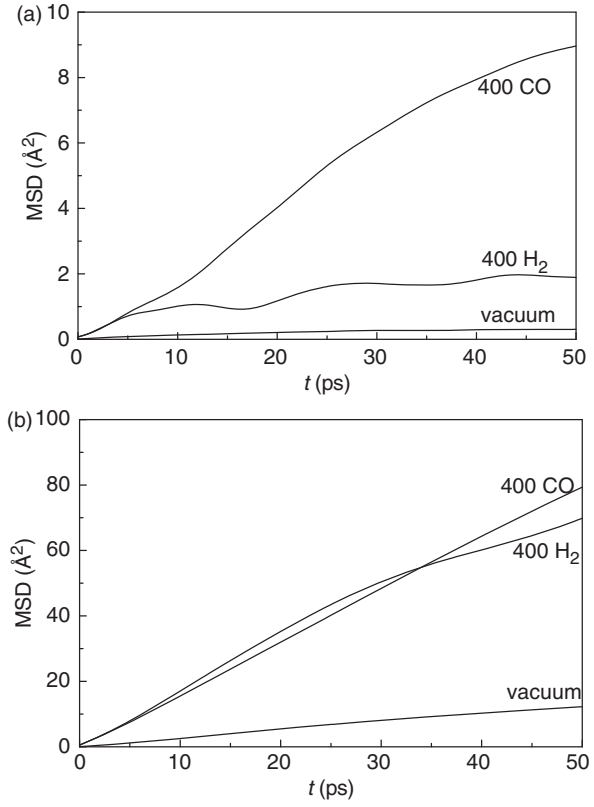

Figure 12. Mean square displacement for the Cu atoms as a function of simulation time in different conditions at (a) 200 K, and (b) 800 K.

(diffusivity $= 5.40 \times 10^{-7}\,\mathrm{cm^2\,s^{-1}}$) in vacuum. The plot obtained in the presence of H_2 and CO molecules lie above it, with larger slopes of 3.29×10^{-6} and $1.98 \times 10^{-5}\,\mathrm{cm^2\,s^{-1}}$, respectively. However, in the case of H_2 gas, there is a smaller difference with vacuum than CO gas. According to the adsorption isotherms (Figure 9), at low temperatures the amount of adsorbed CO molecules is higher than H_2 molecules, and so these molecules have greater impact on the motion of Cu atoms. At 800 K, which is above the nanocluster's melting point, the values of MSD and diffusivities are much higher (note the difference in the scales of the diagrams) for all three cases. The diffusion constant at 800 K for the cluster in vacuum, H_2, and CO atmosphere are 5.23×10^{-5}, 1.42×10^{-4}, and $1.61 \times 10^{-4}\,\mathrm{cm^2\,s^{-1}}$, respectively. At this temperature, the cluster is molten and the pressure exerted by gas molecules increases the overall diffusivity of the cluster. The difference between the CO and H_2 environments is very small in this case. It seems that the nature of gas molecules doesn't have a noticeable impact on the atomic motions at such a high temperature. These observations are in agreement with previous findings [15].

4. Conclusions

In this paper, we explained the thermodynamic and structural changes in a supported nanocluster during the heating and cooling processes, and the effect of gas molecules on it. These properties depend on the cluster size and temperature. Here, we have changed the temperature in the range 200–1800 K, using a fixed cluster size. The well-known phenomena in melting clusters, such as surface melting and wetting were observed using the density profiles and bond order parameters. The irreversibility of structural changes with respect to temperature was also shown. In the study of gas adsorption, CO molecules were shown to adsorb more, and to have more effect on the cluster shape and diffusion constant than H_2. These results justify the application of classical molecular dynamics simulations to study metal clusters. The results of this study are important for the processes of electrochemistry, catalysis, and corrosion.

Acknowledgements

Computations were performed on the gpc supercomputer at the SciNet HPC Consortium. SciNet is funded by: the Canada Foundation for Innovation under the auspices of Compute Canada; the Government of Ontario; Ontario Research Fund – Research Excellence; and the University of Toronto.

References

[1] C.R. Henry, Surf. Sci. Rep. **31**, 231 (1998).
[2] F. Baletto and R. Ferrando, Rev. Modern Phys. **77**, 371 (2005).
[3] Z.-M. Wu, X.-Q. Wang and Y.-Y. Yang, Chin. Phys. **16**, 405 (2007).
[4] H. Lei, J. Phys.: Condens. Matter **13**, 3023 (2001).
[5] S.-P. Huang and P.B. Balbuena, Mol. Phys. **100**, 2165 (2002).
[6] S.-P. Huang, D.S. Mainardi and P.B. Balbuena, Surf. Sci. **545**, 163 (2003).
[7] P. Jensen, A. Clément and L.J. Lewis, Comput. Mater. Sci. **30**, 137 (2004).
[8] J.C. Jiménez-Sáez, A.M.C. Pérez-Martín and J.J. Jiménez-Rodríguez, Nucl. Instrum. Meth. B **249**, 816 (2006).
[9] C.F. Sanz-Navarro, P.-O. Åstrand, D. Chen, M. Rønning, A.C.T. van Duin, J.E. Mueller and W.A. Goddard III, J. Phys. Chem. C **112**, 12663 (2008).
[10] L.M. Gassa, A.M.C. Luna, R.M.T. Sánchez and J.O. Zerbino, Portugaliae Electrochim. Acta **22**, 81 (2004).
[11] P.L. Hansen, J.B. Wagner, S. Helveg, J.R. Rostrup-Nielsen, B.S. Clausen and H. Topsøe, Science **295**, 2053 (2002).

[12] M.J.S. Spencer and G.L. Nyberg, Mol. Simulat. **28**, 807 (2002).
[13] J. Wang, S. Funk and U. Burghaus, Catal. Lett. **103**, 219 (2005).
[14] G.-W. Wu and K.-Y. Chan, J. Electroanal. Chem. **450**, 225 (1998).
[15] E.J. Lamas and P.B. Balbuena, J. Phys. Chem. B **107**, 11682 (2003).
[16] A.P. Sutton and J. Chen, Philos. Mag. Lett. **61**, 139 (1990).
[17] H.J. Hwang, O.-K. Kwon and J.W. Kang, Solid State Commun. **129**, 687 (2004).
[18] X. Zhang and W. Wang, Fluid Phase Equilib. **194–197**, 289 (2002).
[19] F. Huarte-Larrañaga and M. Alberti, Chem. Phys. Lett. **445**, 227 (2007).
[20] A. Sirjoosingh, S. Alavi and T.K. Woo, J. Phys. Chem. C **114**, 2171 (2010).
[21] W. Smith and T.R. Forester, *DL_POLY* (Daresbury Laboratory, Daresbury, 1996).
[22] D.J. Evans, J. Chem. Phys. **78**, 3297 (1983).
[23] D. van der Spoel, E. Lindahl, B. Hess, A.R. van Buuren, E. Apol, P.J. Meulenhoff, D.P. Tieleman, A.L.T.M. Sijbers, K.A. Feenstra, R. van Drunen and H.J.C. Berendsen, Gromacs User Manual version 4.0, www.gromacs.org (2005).
[24] H. Reiss, P. Mirabel and R.L. Whetten, J. Phys. Chem. **92**, 7241 (1988).
[25] S.K.R.S. Sankaranarayanan, V.R. Bhethanabotla and B. Joseph, Phys. Rev. B **71**, 195415 (2005).
[26] Z.L. Wang, J.M. Petroski, T.C. Green and M.A. El-Sayed, J. Phys. Chem. B **102**, 6145 (1998).
[27] P.J. Steinhardt, D.R. Nelson and M. Ronchetti, Phys. Rev. B **28**, 784 (1983).
[28] Y. Wang, S. Teitel and C. Dellago, J. Chem. Phys. **122**, 214722 (2005).
[29] S.K.R.S. Sankaranarayanan, V.R. Bhethanabotla and B. Joseph, Phys. Rev. B **72**, 195405 (2005).
[30] P.B. Balbuena and K.E. Gubbins, Langmuir **9**, 1801 (1993).